

Cite this: *J. Mater. Chem. A*, 2014, 2, 14228

Influence of mono *versus* bis-electron-donor ancillary ligands in heteroleptic Ru(II) bipyridyl complexes on electron injection from the first excited singlet and triplet states in dye-sensitized solar cells†

Hammad Cheema,^a Ashraful Islam,^b Liyuan Han,^b Bhoj Gautam,^c Robert Younts,^c Kenan Gundogdu^c and Ahmed El-Shafei^{*a}

A novel heteroleptic Ru(II) bipyridyl complex (HD-1-mono) was molecularly designed with a mono-carbazole ancillary ligand, synthesized and characterized for DSCs. The aim was to systematically study the influence of mono (HD-1-mono) *versus* bis-carbazole ancillary ligand (NCSU-10) on molar absorptivity, light harvesting efficiency (LHE), ground and excited state oxidation potentials, incident-photon-to-current conversion efficiency (IPCE), electron injection from the first excited singlet and triplet states, short-circuit photocurrent density (J_{sc}), and total solar-to-electric conversion efficiency (η) for DSCs. This study showed that HD-1-mono exhibited slightly lower V_{oc} but greater J_{sc} compared to NCSU-10. Though HD-1-mono showed lower extinction coefficient than NCSU-10, interestingly, it was found that the decrease in molar extinction coefficient of HD-1-mono is not directly related to the short-circuit photocurrent density (J_{sc}). For example, HD-1-mono showed a higher J_{sc} of 21.4 mA cm⁻² without the presence of any additives. However, under optimized conditions, HD-1-mono showed a J_{sc} of 19.76 mA cm⁻², V_{oc} of 0.68 V, and ($\% \eta$) of 9.33 compared to a J_{sc} of 19.58 mA cm⁻², V_{oc} of 0.71 and ($\% \eta$) of 10.19 for NCSU-10, where N719 achieved a J_{sc} of 16.85 mA cm⁻², V_{oc} of 0.749 V and ($\% \eta$) of 9.33 under the same experimental device conditions. Impedance results for HD-1-mono showed a shorter recombination time as compared to N719 and NCSU-10, which justify its lower V_{oc} . Femtosecond transient absorption spectroscopy results elucidated that electron injection from the first triplet state is 63% more efficient for HD-1-mono than that of NCSU-10.

Received 19th April 2014

Accepted 4th June 2014

DOI: 10.1039/c4ta01942c

www.rsc.org/MaterialsA

1. Introduction

Dye-sensitized solar cells (DSCs) are unique compared to silicon-based solar cells in many ways. For examples, DSCs are made of inexpensive materials, their manufacturing is cost effective and flexible, can be made in different colors and exhibit superior performance in rainy, diffused and year around conditions.¹⁻⁹ Owing to the aforementioned unique features, different components of DSCs such as sensitizers, TiO₂ and redox shuttles have been widely studied and improved during the last two decades.^{7,8,10-13} Sensitizers are one of the most critical components within DSCs and Ru(II) based sensitizers

have continuously shown greater than 10% (ref. 5 and 14-18) over-all power conversion efficiency. Among the Ru(II) polypyridyl complexes N719 (11.18%)¹⁹ is a popular benchmark dye both in academia and in industry. However, strategies are needed to improve the NIR response of Ru(II) sensitizers, such as increase in molar absorptivity and fine tuning of ground and excited state oxidation potentials. The goal is to molecularly engineer a panchromatic sensitizer which not only absorbs most of the energetic photons in the range of 400 nm to 920 nm but also maintains favorable thermodynamic ground and excited state oxidation potentials for dye regeneration and electron injection, respectively, which would ultimately result in an ideal sensitizer with minimum recombination losses.

With the aforementioned in mind, this work is focused on the molecular modulations of a previously reported highly efficient Ru(II) based sensitizer known as NCSU-10 (ref. 5) as shown in Fig. 1. Our strategy was to use one carbazole ancillary ligand, HD-1-mono (Fig. 1), to reduce the molecular size and study how that influences the light harvesting efficiency, electron injection from the first excited singlet and triplet states,

^aPolymer and Color Chemistry Program, North Carolina State University, Raleigh, NC, 27695, USA. E-mail: Ahmed_El-Shafei@ncsu.edu

^bPhotovoltaic Materials Unit, National Institute for Materials Science, 1-2-1 Sengen, Tsukuba, Ibaraki 305-0047, Japan

^cPhysics Department, North Carolina State University, Raleigh, NC, 27695, USA

† Electronic supplementary information (ESI) available: Synthesis details, FT-IR, ¹H-NMR and CV graphs. See DOI: 10.1039/c4ta01942c

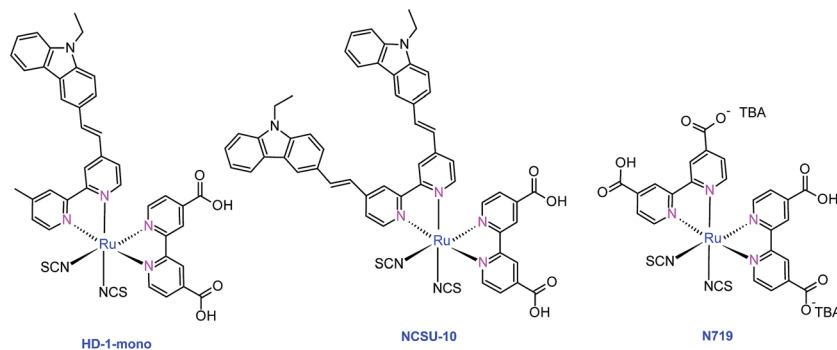


Fig. 1 Molecular structures of complexes HD-1-mono, NCSU-10 and N719.

photovoltage, sensitizer redox properties, decay dynamics and the charge separation/recombinations at the dye–TiO₂–electrolyte interfaces. Similar ideas have been reported previously for sensitizers JK-56 (ref. 20) and D-20.²¹ In both cases mono-based sensitizers resulted in higher current and overall greater efficiency than the bis-ancillary ligand analogs due to decreased loading for bis analogs. However in both JK-56 and D-20, the ancillary ligands were of much larger molecular size compared to carbazole, thus the molecular size is expected to have minimal influence in this study. To better understand the origin of higher J_{sc} in HD-1-mono compared to NCSU-10 and N719, TiO₂–dye interface properties were studied by impedance spectroscopy which is directly correlated with photocurrent and photovoltage. Time-correlated single photon counting (TCSPC) and ultra-fast transient absorption measurements were performed to understand the fundamental difference in the photo-physics and electron injection properties of HD-1-mono and NCSU-10 in solar cell form. UV-Vis, fluorescence, and cyclic voltammetry measurements were performed to ascertain the difference in molar absorptivity, excited state and redox properties of HD-1-mono and NCSU-10, respectively. The goal is to understand the fundamental difference between HD-1-mono and NCSU-10 for the design of more efficient sensitizers, both in terms of higher photocurrent and photovoltage for DSCs.

2. Results and discussion

The synthesis of the proposed sensitizer HD-1-mono was carried out in a similar way to that reported for NCSU-10 (ref. 5 and 22) using a 1 : 1 molar ratio of 4,4'-dimethyl-2,2'-bipyridine to 9-ethyl-9H-carbazole-3-carbaldehyde. HD-1-mono was synthesized in the typical one-pot three-step synthetic scheme as shown in the ESI.† The typical raw product yield was up to 90%, which was then run through a Sephadex LH-20 column three times to get the highly pure product in 55% yield.

2.1. Photophysical measurements

A comparison between the UV-Vis absorption and emission spectra of N719, HD-1-mono, and NCSU-10 is given in Fig. 2, and the results are summarized in Table 1.

An intense MLCT absorption peak was found for HD-1-mono at 538 nm ($15\,550\text{ M}^{-1}\text{ cm}^{-1}$) compared to NCSU-10 at 545 nm

($20\,650\text{ M}^{-1}\text{ cm}^{-1}$) and N719 at 529 nm ($12\,800\text{ M}^{-1}\text{ cm}^{-1}$). HD-1-mono showed slightly blue shifted spectra and up to 30% decrease in extinction coefficient compared to NCSU-10. However, extended π -conjugation and a stronger electron donating carbazole ancillary ligand resulted in destabilized metal based HOMO (t_{2g}) and red shifted absorption spectra, compared to N719, due to the decreased HOMO–LUMO gap, as shown in the energy level diagram of Fig. 3. Emission λ_{max} for HD-1-mono was also blue shifted compared to that of NCSU-10 and N719.

In terms of ancillary ligands itself, there was no substantial change in optical and electrochemical properties (ESI Fig. 8–10S†) for HD-1-mono and NCSU-10, as observed by UV-Vis, emission and cyclic voltammetry. Thus molecular modulation of ancillary ligands was expected to have a negligible effect on optical and electrochemical properties of the corresponding complexes.

2.2. Electrochemical measurements

The ground state oxidation potential (GSOP) of HD-1-mono was measured in two ways. First, by cyclic voltammetry (CV) in solution form, and the second by using a photoemission yield spectrometer (Riken Keiki AC-3E), while the dye anchored to the TiO₂ film. The results are summarized and compared in Table 2. It was observed that while anchored to TiO₂, the GSOP of both dyes shifted negatively owing to de-protonation of complexes. CV graphs were used to calculate the oxidation onset which is equivalent to the GSOP (ground state oxidation potential) or HOMO level of the dye. Additionally, E_{0-0} was calculated from the intersection point of experimental absorption and emission spectra and can be defined as the difference between the excited and ground state oxidation potentials. Then values of E_{0-0} and GSOP were used to calculate the ESOP (excited state oxidation potential) or LUMO level of the dye, the values in volts (V) vs. NHE were converted to electron volt (eV) as shown in eqn (1).

$$\text{ESOP} = (\text{GSOP} + 4.7) - E_{0-0} \quad (1)$$

The GSOP value of -5.46 for HD-1-mono confirmed that the HOMO of this dye is below the I_3^-/I^- redox couple (-5.2 eV),²³ and the difference is large enough for electron replenishment

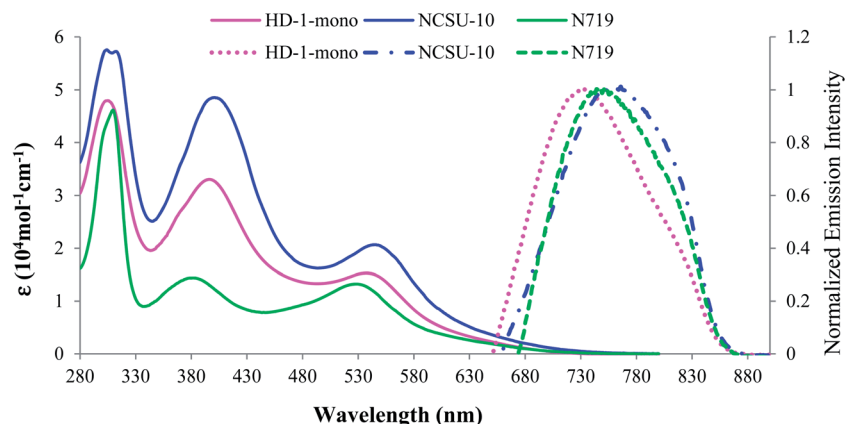


Fig. 2 UV-Vis absorption (solid-line) and emission spectra (dashed-line) of complexes HD-1-mono as compared to N719 and NCSU-10 measured in DMF (2×10^{-5} M).

Table 1 Absorption and emission properties for HD-1-mono as compared to NCSU-10 and N719

Sensitizer	Absorption λ_{\max} (nm)	ϵ ($M^{-1} \text{ cm}^{-1}$)	Emission λ_{\max} (nm)
HD-1-mono	304, 396, 538 (d \rightarrow π^*)	51 900; 33 350; 15 550	728
NCSU-10	304, 401, 545 (d \rightarrow π^*)	57 550; 48 555; 20 650	758
N719	310, 381, 529 (d \rightarrow π^*)	46 100; 14 400; 12 800	744

and efficient dye regeneration. Additionally, the ESOP energy level of HD-1-mono was at -3.55 eV which was above the conduction band edge of nanocrystalline TiO_2 (-4.2 eV).²⁴ Similar measurements for NCSU-10 showed that GSOP is at -5.5 eV and ESOP at -3.57 eV thus resulting in favorable dye regeneration and electron injection, respectively. Thus owing to the energetically favorable excited states, the efficient electron injection into the CB edge of TiO_2 and dye regeneration was achieved with sensitizers HD-1-mono. According to the energy level diagram in Fig. 3, the HOMO destabilization is in the order

of HD-1-mono > NCSU-10 > N719, which is consistent with the order of experimental J_{sc} of HD-1-mono > NCSU-10 > N719.

Similar Ru(II) complexes have been recognized to have electron injection both from singlet and triplet energy states,^{8,26-28} thus it was important to estimate whether the molecular modulation of the mono *versus* bis-ancillary ligands invokes direct changes in electron injection from singlet and triplet states and in their energy values. Singlet and triplet energy levels were estimated from the onset of fluorescence (E_{0-0} , Fig. 2) and phosphorescence (ESI Fig. 13S[†]) emission. It was found that HD-1-mono and NCSU-10 have singlet at -3.55 eV, -3.57 eV and triplet energy levels at -4.1 eV and -4.14 eV, respectively. Triplet energy levels were approximately 0.55 eV and 0.57 eV lower than singlet energy levels of HD-1-mono and NCSU-10, respectively. Thus, the triplet energy level of HD-1-mono is 0.1 eV higher in energy than the TiO_2 (-4.2 eV)²⁴ conduction band compared to 0.06 eV of NCSU-10. Hence, because of the more free energy of the triplet level for HD-1-mono, more triplet electron injection was expected than that of NCSU-10.

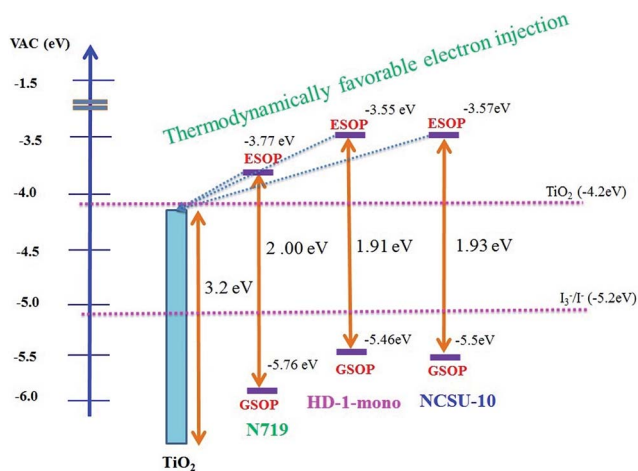


Fig. 3 Energy level diagram and comparison between GSOP and ESOP of N719, HD-1-mono and NCSU-10.

2.3. Photovoltaic device characterization

The photovoltaic performance of complexes HD-1-mono, NCSU-10 and N719 on the nanocrystalline TiO_2 electrode was studied under standard AM 1.5 irradiation (100 mW cm^{-2}) using an electrolyte with a composition of 0.6 M dimethylpropyl-imidazolium iodide (DMPII), 0.05 M I_2 , and 0.1 M LiI in acetonitrile. Fig. 4 shows the incident-photon-to-current efficiency conversion (IPCE) spectra for the cells fabricated with complexes HD-1-mono, NCSU-10, and N719, where the incident photon-to-

Table 2 The excited state oxidation potential (E^*) and the lowest singlet-singlet electronic transitions (E_{0-0}) for ligands and HD-1-mono compared to NCSU-10 and N719^a

Sensitizer	Experimental (eV)			E^*
	$^*E_{0-0}$	\heartsuit GSOP(HOMO)	\heartsuit^* GSOP(HOMO)	
		(CV)	(AC3)	
LH-1-mono	2.94	-5.65	—	-2.71
L-NCSU-10	2.94	-5.66	—	-2.72
HD-1-mono	1.91	-5.46	-5.38	-3.55
NCSU-10	1.93	-5.50	-5.50	-3.57
N719	1.99	-5.76	-5.76	-3.77

^a * E_{0-0} = calculated from the intersection point of experimental absorption and emission spectra (DMF); \heartsuit GSOP = ground state oxidation potential = E_{HOMO} ; \heartsuit^* GSOP was measured in DMF with 0.1 M [TBA][PF6] and with a scan rate of 50 mV s⁻¹. It was calibrated with Fc/Fc⁺ as an internal reference and converted to NHE by addition of 0.63 V; \heartsuit^* GSOP was also measured using a photoemission yield spectrometer (Riken Keiki AC-3E); excited-state oxidation potential, E^* was calculated from: $E^* = \text{GSOP} - ^*E_{0-0}$. Calculated GSOP, ESOP, and E_{0-0} of N719 were reported elsewhere.^{5,25} GSOP and ESOP for the ligands were calculated using the same method used for the dyes.

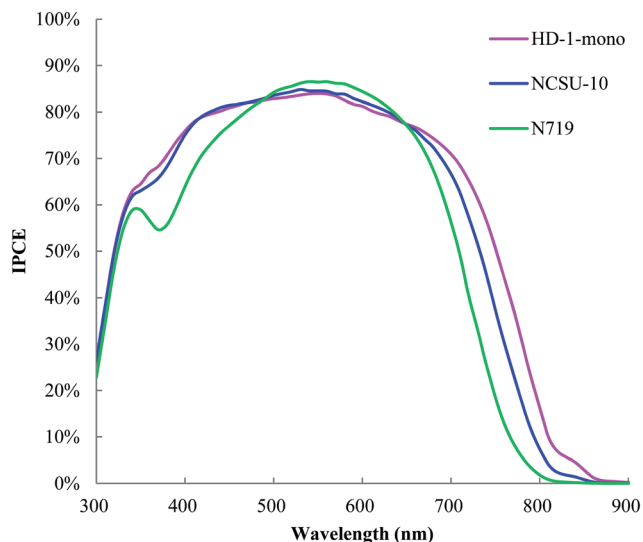


Fig. 4 Photocurrent action spectra (IPCE) obtained with dyes HD-1-mono, NCSU-10 and N719 anchored to the nanocrystalline TiO₂ film.

current conversion efficiency (IPCE) values are plotted as a function of wavelength.

Fig. 4 shows the impressive photocurrent response of carbazole based sensitizers HD-1-mono and NCSU-10. HD-1-mono outperformed the benchmark N719 in its photocurrent response owing to strong photon harvesting characteristics of the carbazole based ancillary ligand. The presence of only one (mono) carbazole did not affect the IPCE negatively, compared to NCSU-10 (bis). In fact, HD-1-mono showed better response than NCSU-10 particularly in the redder portion of the spectrum.

The photovoltaic parameters including the short-circuit photocurrent density (J_{sc}), open-circuit voltage (V_{oc}), fill factors (FF) and overall cell efficiencies (η) are summarized in Table 3.

Table 3 Photovoltaic characteristics of HD-1-mono, NCSU-10 and N719^a

Sensitizer	TBP (M)	J_{sc} (mA cm ⁻²)	V_{oc} (V)	FF	η (%)
HD-1-mono	0.0	21.40	0.55	0.60	7.06
	0.5	19.76	0.68	0.694	9.33
NCSU-10	0.5	19.58	0.713	0.73	10.19
N719	0.5	16.85	0.749	0.739	9.33

^a Conditions: sealed cells; coadsorbate, DCA 20 mM; photoelectrode, TiO₂ (15 μm thickness and 0.25 cm²); electrolyte, 0.6 M DMPII, 0.1 M LiI, 0.05 I₂ in AN; irradiated light, AM 1.5 solar light (100 mW cm⁻²). J_{sc} , short-circuit photocurrent density; V_{oc} , open-circuit photovoltage; FF, fill factor; η , total power conversion efficiency.

The solar cell sensitized with HD-1-mono showed an impressively higher short-circuit photocurrent density (J_{sc}) of 21.4 mA cm⁻², an open-circuit photovoltage (V_{oc}) of 0.55 V, and a fill factor of 0.60, corresponding to an overall conversion efficiency (η) of 7.06 without any additives. The J_{sc} of 21.4 mA cm⁻², which is 21% higher than the J_{sc} of N719 is likely due to efficient photon harvesting and more energetically favorable electron injection into TiO₂ from the first excited triplet. An addition of 0.5 M TBP resulted in a J_{sc} of 19.76 mA cm⁻², a V_{oc} of 0.68 V and a total conversion efficiency (η) of 9.33 for the HD-1-mono based solar cell. The impressive increase in V_{oc} and the overall efficiency in the presence of TBP is likely due to the reduction of recombination between the injected electron and electrolyte at TiO₂-dye-electrolyte interfaces, owing to the formation of a protecting layer of TBP.⁵ The upward shift in the TiO₂ conduction band edge and an increase in electron lifetime were also reported to be caused by the presence of TBP.⁸ Thus based on current-voltage results, it can be said that the attempted molecular modulation resulted in higher J_{sc} at the expense of a decrease in photovoltage, which is most likely caused by dark current or recombination reactions.

Under similar conditions, HD-1-mono exhibited slightly lower V_{oc} than NCSU-10, which contradicts with previous findings^{20,21} of lower V_{oc} in the case of bis-ancillary ligand vs. mono analogs. Choi *et al.*²⁰ and Jung *et al.*²¹ noticed a decrease in loading for bis compared to mono-antenna based sensitizers. Our molecular design strategy circumvented this situation by employing a highly efficient and small sized carbazole-based ancillary ligand.

2.4. Electrochemical impedance spectroscopy characterization

Electrochemical impedance spectroscopy (EIS) is a key technique to study the electrical energy storage and dissipative properties of passive electrical systems. Impedance is different from resistance in that it also takes care of the dynamic processes such as relaxations related to dielectric and charge transfer between heterogeneous surfaces. In DSCs, EIS is a powerful tool in characterizing the interfacial charge transfer process at TiO₂-electrolyte and pt-electrolyte interfaces.^{22,29} The EIS Nyquist and Bode plots for the DSCs based on HD-1-mono, NCSU-10 and N719 are shown in Fig. 6 and 7, respectively. In

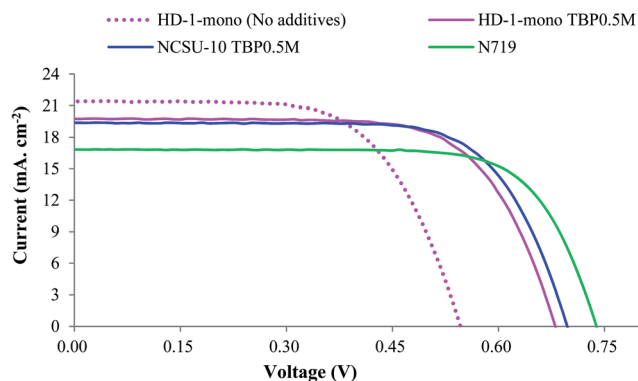


Fig. 5 Photocurrent voltage characteristics of DSCs sensitized with the complexes HD-1-mono, NCSU-10 and N719 electrolyte, 0.6 M DMPII, 0.1 M LiI, and 0.05 I₂ in acetonitrile (AN), whereas TBP (*tert*-butylpyridine) was added as an additive in the dye solution.

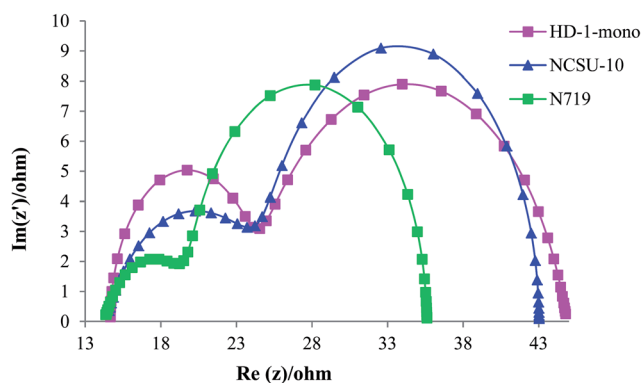


Fig. 6 EIS Nyquist plots for DSCs sensitized with HD-1-mono, NCSU-10, and N719.

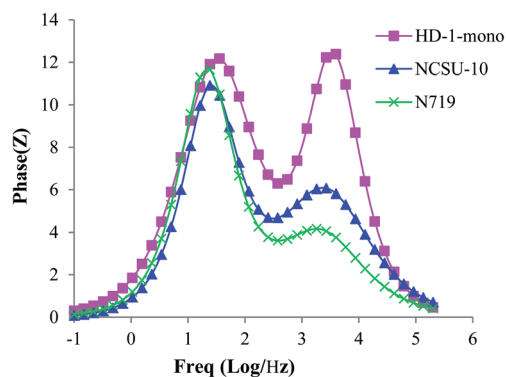


Fig. 7 EIS Bode plots for DSCs sensitized with, HD-1-mono, NCSU-10 and N719.

EIS Nyquist plots, the radius of the bigger semicircle shows the electron recombination resistance at the TiO₂/dye/electrolyte interface, which was the highest for NCSU-10 compared to HD-1-mono and N719.

In Fig. 7, the frequency response in the range of 0-2.5 Log/Hz is indicative of the recombination between electrolyte and eTiO₂ (electrons which are injected in TiO₂ CB), which is related to the

electron lifetime in the CB of TiO₂. The middle-frequency (0-2.5 Log/Hz on *x*-axis) peaks of the DSCs based on NCSU-10 and N719 were shifted to lower frequency relative to that of HD-1-mono, indicating a shorter recombination lifetime for the latter case, thus resulting in lower *V*_{oc} for HD-1-mono as compared to NCSU-10 and N719. EIS results clearly demonstrated qualitatively that in the case of HD-1-mono, the injected electrons are prone to recombine due to the shorter lifetime in the TiO₂ CB. The shorter eTiO₂ lifetime for HD-1-mono can be attributed tentatively to the decrease in the hydrophobicity of the mono *versus* bis which resulted in decrease in the insulating property of the dye towards charge recombinations at the TiO₂-I₃⁻ interface compared to NCSU-10. Similar results of a longer eTiO₂ lifetime for carbazole based dyes were related to the density of alkyl chains present which block the access of I₃⁻ or cations to the TiO₂ surface.^{30,31} However, owing to the complexity of charge transfer process in DSCs, full electrochemical characterization is recommended to completely understand the charge transfer at the interface of HD-1-mono/TiO₂ compared to that of NCSU-10/TiO₂ and N719/TiO₂.

2.5. Time correlated single photon counting (TCSPC) spectroscopy measurements

The TCSPC spectroscopy method was employed to study the excited state lifetime and emission decay behavior of the dyes in solution and in cell form (DSC). The inset of Fig. 8 shows the excited state decay behavior of the dyes in DMF. All of the decay curves were fitted with 2-exponential showing the multi-exponential decay behavior having fast (shorter lifetime) and slow (longer lifetime) components. The relative amplitude of the fast component (B1) for HD-1-mono and NCSU-10 was substantially different from that of N719. The reported value of the excited state lifetime for N719 in air saturated ethanol solution is 40 ns,¹ but in our case, it was 38 ns in DMF. HD-1-mono and NCSU-10 exhibited the excited state lifetime of 85 ns and 59 ns, respectively as given in Table 4.

However, when the decay behaviors were studied by the TCSPC technique^{32,33} on the complete DSC, the decay rate was in the following order HD-1-mono > NCSU-10 > N719 as shown in Fig. 8. TCSPC decay behavior was consistent with the photocurrent response of dyes in DSCs. Hence it can be postulated that faster decay is the result of reduced kinetic redundancy of the excited state owing to the optimized excited state lifetime as found by Durrant *et al.*³³ which leads to efficient electron injection, resulting in higher photocurrent for HD-1-mono, which is consistent with the shorter eTiO₂ lifetime as found from EIS measurements.

2.6. Femtosecond transient absorption spectroscopy measurements

To understand the differences in *J*_{sc} and *V*_{oc} (Fig. 5) of the devices as a function of electron-donor ancillary ligands, femtosecond transient absorption spectroscopy (TAS) was performed to understand the fundamental excited state dynamics by measuring the charge separation dynamics at the dye-TiO₂ interface. Fig. 9a and b show the transient absorption spectra

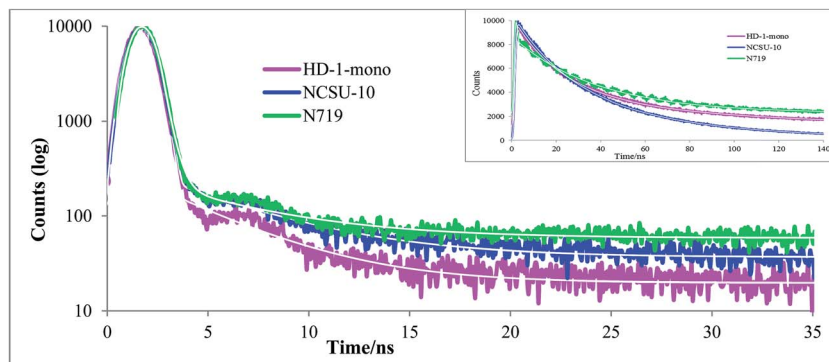


Fig. 8 Excited state decay behaviors of HD-1-mono, NCSU-10 and N719 in the complete cell, (inset) in solution dyes dissolved in DMF, studied using the TCSPC method, smooth lines correspond to the fits of the experimental data after convolution with the instrument response.

Table 4 Excited state lifetime in solution form

Sample name	τ/ns (T_1)	τ/ns (T_2)
HD-1-mono	21 ($^a B_1 = 32$)	85 ($B_2 = 68$)
NCSU-10	25 ($B_1 = 34$)	59 ($B_2 = 66$)
N719	0.1 ($B_1 = 3$)	38 ($B_2 = 97$)

^a B denotes the relative amplitude of each component.

for these dyes at 0 ps and 500 ps as an example. It consists of ground state bleaching (GSB) with increased transmission above 2.0 eV (<620 nm) and the flat photo-induced absorption (PIA) band below 2.0 eV (>620 nm) for both samples.

Previous studies on similar Ru(II) based DSCs revealed that the PIA spectrum is sensitive to the charge separation dynamics as it probes the oxidized form of dye (dye^+), excited state dye (dye^*) and injected electrons into TiO_2 ($e\text{-TiO}_2$).³⁴ The PIA at 680 nm primarily reveals exciton population (dye^*) whereas at 770 nm, PIA reveals oxidized dye (dye^+) population.³⁵ Therefore comparison of the time evolution of these two spectral locations reveals a complementary picture of exciton lifetime and charge injection from the dye into TiO_2 .^{33,35-41}

Fig. 10 shows the evolution of the PIA feature at 680 nm and 770 nm, in samples without electrolyte. For both samples, the very fast rise at both 680 nm and 770 nm suggests an impulsive exciton creation and immediate charge injection. On the other hand, for both samples, 770 nm data decays much slower compared to 680 nm.

Table 5 shows the comparison of the decay on two devices at 680 nm and 770 nm for each dye, HD-1-mono and NCSU-10. These data agree with the assessment that 680 nm probes primarily dye^* and 770 nm probes dye^+ . Because the dye^* population decays through both recombination and charge injection into TiO_2 ($\text{ESI } 11\text{S}-12\text{S}^\dagger$).

The addition of electrolyte completely changes the dynamics. As shown in Fig. 11a and b the dynamics in 680 nm and 770 nm evolves in a different pace. In contrast to the sharp, fast rise and then slower decay at 680 nm, the dynamics at 770 nm exhibits a two-step growth process with sharp and slow components, which takes place over a longer period of time. For

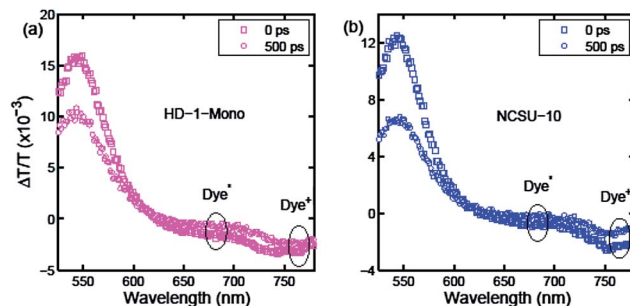


Fig. 9 Transient absorption spectra at $t = 0$ ps and $t = 500$ ps of (a) HD-1-mono and (b) NCSU-10 with the electrolyte. Dye^* and dye^+ represent the majority of excited dye and oxidized dye population respectively.

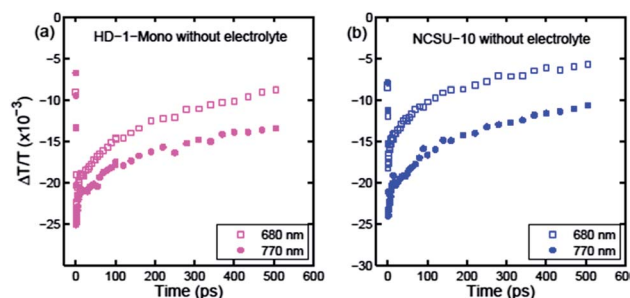


Fig. 10 PIA decay dynamics of (a) HD-1-mono and NCSU-10 without electrolyte and (b) NCSU-10 without electrolyte. Colors are indicated in the legend.

NCSU-10, this slow rise saturates in the first 20 ps. However, for HD-1-mono, it saturates at a later time of about 150 ps at greater amplitude. The saturation of growth of the slow component at 20 ps in NCSU-10 compared to that at 150 ps in HD-1-mono indicates that in the HD-1-mono device, the charge injection continues for a longer time and is more efficient compared to that from NCSU-10.³⁶

The comparison in these spectral evolutions in the two DSC structures clearly shows the difference in charge separation dynamics. In both samples, charge injection from the singlet

Table 5 Comparison of decay of two devices for each dye, one at 680 nm and the other at 770 nm^a

Sample name	Wavelength (nm)	τ/ps (T_1)	τ/ps (T_2)	τ/ps (T_3)
HD-1-mono	680	3.5 ps ($B_1 = 22\%$)	89 ps ($B_2 = 22\%$)	1014 ps ($B_3 = 56\%$)
HD-1-mono	770	3.6 ps ($B_1 = 17\%$)	136 ps ($B_2 = 22\%$)	2594 ps ($B_3 = 61\%$)
NCSU-10	680	3.3 ps ($B_1 = 16\%$)	76 ps ($B_2 = 30\%$)	945 ps ($B_3 = 54\%$)
NCSU-10	770	4.3 ps ($B_1 = 16\%$)	126 ps ($B_2 = 27\%$)	1730 ps ($B_3 = 57\%$)

^a B denotes the relative amplitude of each component.

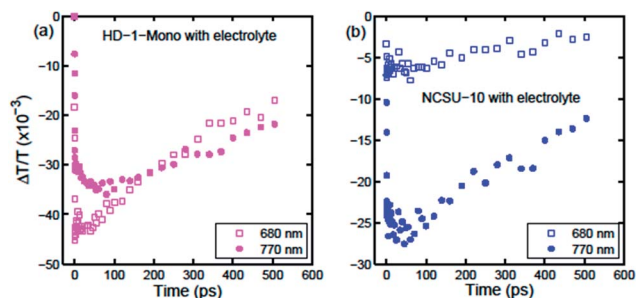


Fig. 11 PIA decay dynamics of (a) HD-1-mono (b) NCSU-10 with the electrolyte. Colors are indicated in the legend.

states is very similar. With the addition of electrolyte, the Fermi level for the TiO_2 band and trap states shifts,³³ which facilitates electron injection from the triplet state of the dyes. These data confirmed that triplet state injection is more efficient in HD-1-mono than in NCSU-10. In order to quantify the difference between the triplet state injections between the two dyes, we normalized the decay of 770 nm signal in the samples with and without the electrolyte. Since the electrolyte addition primarily enhances the injection from the triplet state, we subtracted these two signals to find the relative increase in the triplet injection in both dyes. The results are displayed in Fig. 12. The comparison of signal maxima in Fig. 12 suggests 63% higher

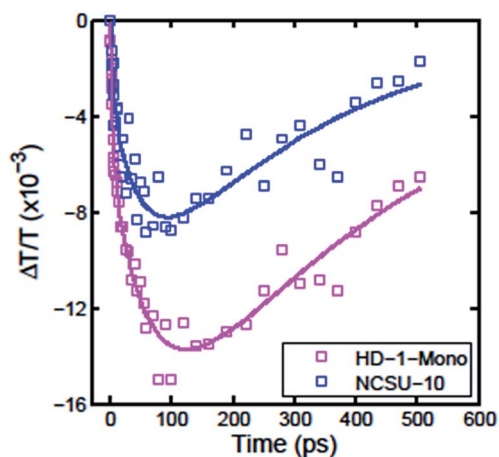


Fig. 12 Comparison of triplet injection on HD-1-mono and NCSU-10. Solid lines refer to the fitting with three exponentials.

electron injection efficiency from the triplet state in HD-1-mono compared to NCSU-10. This increase is consistent with greater J_{sc} as observed for HD-1-mono. However, these data also suggest that not all of the injected charges are converted into current likely due to small negative free energy, which can be fine-tuned to enhance the efficiency of triplet injection.

3. Conclusions

The molecular modulation of bis-carbazole (NCSU-10) to mono-carbazole (HD-1-mono) resulted in higher photocurrent response and favorable redox properties. Comparison of the photovoltaic, electrochemical and optical properties revealed that the number of ancillary ligands can have a significant effect on the solar cell performance. Our findings showed that the V_{oc} of the mono *versus* bis contradicts the previous findings of lower V_{oc} for bis analogs, owing to superior photon harvesting and small molecular size of carbazole without sacrificing the solar to power conversion efficiency of solar cells. It was also found that HD-1-mono shows 63% more favored electron injection from the triplet state compared to NCSU-10 as shown by femtosecond transient absorption spectroscopy experiments. Results from TCSPC of excited state decay rates were consistent with femtosecond TAS. EIS showed that HD-1-mono offers lower recombination resistance on the TiO_2 surface compared to NCSU-10, and the injected electrons have a shorter lifetime in TiO_2 , resulting in higher recombination and lower V_{oc} . We believe this strategy will greatly help in future design of efficient sensitizers both in terms of higher photocurrent and photovoltage for DSCs.

References

- 1 M. K. Nazeeruddin, S. M. Zakeeruddin, R. Humphry-Baker, M. Jirousek, P. Liska, N. Vlachopoulos, V. Shklover, C. Fischer and M. Grätzel, *Inorg. Chem.*, 1999, **38**, 6298–6305.
- 2 P. Péchy, T. Renouard, S. M. Zakeeruddin, R. Humphry-Baker, P. Comte, P. Liska, L. Cevey, E. Costa, V. Shklover, L. Spiccia, G. B. Deacon, C. A. Bignozzi and M. Grätzel, *J. Am. Chem. Soc.*, 2001, **123**, 1613–1624.
- 3 C. Grätzel and S. M. Zakeeruddin, *Mater. Today*, 2013, **16**, 11–18.
- 4 S. Zhang, X. Yang, Y. Numata and L. Han, *Energy Environ. Sci.*, 2013, **6**, 1443–1464.

- 5 A. El-Shafei, M. Hussain, A. Atiq, A. Islam and L. Han, *J. Mater. Chem.*, 2012, **22**, 24048–24056.
- 6 B. O'Regan and M. Grätzel, *Nature*, 1991, **353**, 737–740.
- 7 B. E. Hardin, H. J. Snaith and M. D. McGehee, *Nat. Photonics*, 2012, **6**, 162–169.
- 8 A. Hagfeldt, G. Boschloo, L. Sun, L. Kloo and H. Pettersson, *Chem. Rev.*, 2010, **110**, 6595–6663.
- 9 M. Grätzel, *Inorg. Chem.*, 2005, **44**, 6841–6851.
- 10 A. Mishra, M. Fischer and P. Bäuerle, *Angew. Chem., Int. Ed.*, 2009, **48**, 2474–2499.
- 11 S. Ahmad, E. Guillen, L. Kavan, M. Grätzel and M. K. Nazeeruddin, *Energy Environ. Sci.*, 2013, **6**, 3439–3466.
- 12 Y. Yen, H. Chou, Y. Chen, C. Hsu and J. T. Lin, *J. Mater. Chem.*, 2012, **22**, 8734–8747.
- 13 S. Zhang, X. Yang, Y. Numata and L. Han, *Energy Environ. Sci.*, 2013, **6**, 1443–1464.
- 14 M. K. Nazeeruddin, R. Splivallo, P. Liska, P. Comte and M. Grätzel, *Chem. Commun.*, 2003, 1456–1457.
- 15 M. Grätzel, *J. Photochem. Photobiol., A*, 2004, **164**, 3–14.
- 16 M. Hussain, A. El-Shafei, A. Islam and L. Han, *Phys. Chem. Chem. Phys.*, 2013, **15**, 8401–8408.
- 17 Y. Numata, S. P. Singh, A. Islam, M. Iwamura, A. Imai, K. Nozaki and L. Han, *Adv. Funct. Mater.*, 2012, **23**, 1817–1823.
- 18 Y. Chiba, A. Islam, Y. Watanabe, R. Komiya, N. Koide and L. Han, *Jpn. J. Appl. Phys.*, 2006, **45**, L638–L640.
- 19 M. K. Nazeeruddin, F. De Angelis, S. Fantacci, A. Selloni, G. Viscardi, P. Liska, S. Ito, B. Takeru and M. Grätzel, *J. Am. Chem. Soc.*, 2005, **127**, 16835–16847.
- 20 H. Choi, C. Baik, S. Kim, M. Kang, X. Xu, H. S. Kang, S. O. Kang, J. Ko, M. K. Nazeeruddin and M. Grätzel, *New J. Chem.*, 2008, **32**, 2233–2237.
- 21 I. Jung, H. Choi, J. K. Lee, K. H. Song, S. O. Kang and J. Ko, *Inorg. Chim. Acta*, 2007, **360**, 3518–3524.
- 22 A. El-Shafei, M. Hussain, A. Islam and L. Han, *J. Mater. Chem. A*, 2013, **1**, 13679–13686.
- 23 P. Qu and G. J. Meyer, *Langmuir*, 2001, **17**, 6720–6728.
- 24 G. Oskam, B. V. Bergeron, G. J. Meyer and P. C. Searson, *J. Phys. Chem. B*, 2001, **105**, 6867–6873.
- 25 F. De Angelis, S. Fantacci, A. Selloni, M. K. Nazeeruddin and M. Grätzel, *J. Phys. Chem. C*, 2010, **114**, 6054–6061.
- 26 N. A. Anderson and T. Lian, *Coord. Chem. Rev.*, 2004, **248**, 1231–1246.
- 27 S. Ardo and G. J. Meyer, *Chem. Soc. Rev.*, 2009, **38**, 115–164.
- 28 O. V. Prezhdo, W. R. Duncan and V. V. Prezhdo, *Interface, Acc. Chem. Res.*, 2008, **41**, 339–348.
- 29 N. Koide, A. Islam, Y. Chiba and L. Han, *J. Photochem. Photobiol., A*, 2006, **182**, 296–305.
- 30 N. Koumura, Z. Wang, S. Mori, M. Miyashita, E. Suzuki and K. Hara, *J. Am. Chem. Soc.*, 2006, **128**, 14256–14257.
- 31 M. Miyashita, K. Sunahara, T. Nishikawa, Y. Uemura, N. Koumura, K. Hara, A. Mori, T. Abe, E. Suzuki and S. Mori, *J. Am. Chem. Soc.*, 2008, **130**, 17874–17881.
- 32 S. E. Koops and J. R. Durrant, *Inorg. Chim. Acta*, 2008, **361**, 663–670.
- 33 S. A. Haque, E. Palomares, B. M. Cho, A. N. M. Green, N. Hirata, D. R. Klug and J. R. Durrant, *J. Am. Chem. Soc.*, 2005, **127**, 3456–3462.
- 34 M. Juozapavicius, M. Kaucikas, J. J. van Thor and B. C. O'Regan, *J. Phys. Chem. C*, 2013, **117**, 116–123.
- 35 G. Benko, J. Kalliainen, J. Korppi-Tommola, A. P. Yartsev and V. Sundstrom, *J. Am. Chem. Soc.*, 2002, **124**, 489–493.
- 36 A. Furube, Z. Wang, K. Sunahara, K. Hara, R. Katoh and M. Tachiya, *J. Am. Chem. Soc.*, 2010, **132**, 6614–6615.
- 37 R. Katoh, A. Furube, M. Kasuya, N. Fuke, N. Koide and L. Han, *J. Mater. Chem.*, 2007, **17**, 3190–3196.
- 38 S. E. Koops, B. C. O'Regan, P. R. F. Barnes and J. R. Durrant, *J. Am. Chem. Soc.*, 2009, **131**, 4808–4818.
- 39 J. Sibus, G. Burdziaski, J. Karolczak, J. Idogoras, J. A. Anta and M. Ziolek, *Langmuir*, 2014, **30**, 2505–2512.
- 40 Y. Tachibana, J. E. Moser, M. Grätzel, D. R. Klug and J. R. Durrant, *J. Phys. Chem.*, 1996, **100**, 20056–20062.
- 41 J. Teuscher, J. Dacoppet, A. Punzi, S. M. Zakeeruddin, J. Moser and M. Grätzel, *J. Phys. Chem. Lett.*, 2012, **3**, 3786–3790.